Biomass smoke from southern Africa can significantly enhance the brightness of stratocumulus over the southeastern Atlantic Ocean

Zheng Lu[a], Xiaohong Liu[a,b,1], Zhibo Zhang[c,d], Chun Zhao[e], Kerry Meyer[f], Chamara Rajapakshe[c], Chenglai Wu[a,b], Zhifeng Yang[c,d], and Joyce E. Penner[g]

[a]Department of Atmospheric Science, University of Wyoming, Laramie, WY 82071; [b]International Center for Climate and Environment Sciences, Institute of Atmospheric Physics, Chinese Academy of Sciences, Beijing 100029, China; [c]Physics Department, University of Maryland Baltimore County, Baltimore, MD 21250; [d]Joint Center for Earth Systems Technology, University of Maryland Baltimore County, Baltimore, MD 21250; [e]School of Earth and Space Sciences, University of Science and Technology of China, Hefei 230026, China; [f]Climate and Radiation Laboratory, NASA Goddard Space Flight Center, Greenbelt, MD 20771; and [g]Department of Climate and Space Sciences and Engineering, University of Michigan, Ann Arbor, MI 48109

Edited by James Haywood, University of Exeter, Exeter, United Kingdom, and accepted by Editorial Board Member A. R. Ravishankara February 6, 2018 (received for review August 6, 2017)

Marine stratocumulus clouds cover nearly one-quarter of the ocean surface and thus play an extremely important role in determining the global radiative balance. The semipermanent marine stratocumulus deck over the southeastern Atlantic Ocean is of particular interest, because of its interactions with seasonal biomass burning aerosols that are emitted in southern Africa. Understanding the impacts of biomass burning aerosols on stratocumulus clouds and the implications for regional and global radiative balance is still very limited. Previous studies have focused on assessing the magnitude of the warming caused by solar scattering and absorption by biomass burning aerosols over stratocumulus (the direct radiative effect) or cloud adjustments to the direct radiative effect (the semidirect effect). Here, using a nested modeling approach in conjunction with observations from multiple satellites, we demonstrate that cloud condensation nuclei activated from biomass burning aerosols entrained into the stratocumulus (the microphysical effect) can play a dominant role in determining the total radiative forcing at the top of the atmosphere, compared with their direct and semidirect radiative effects. Biomass burning aerosols over the region and period with heavy loadings can cause a substantial cooling (daily mean −8.05 W m^{-2}), primarily as a result of clouds brightening by reducing the cloud droplet size (the Twomey effect) and secondarily through modulating the diurnal cycle of cloud liquid water path and coverage (the cloud lifetime effect). Our results highlight the importance of realistically representing the interactions of stratocumulus with biomass burning aerosols in global climate models in this region.

stratocumulus clouds | biomass burning aerosols | aerosol–cloud interaction

Biomass burning (BB) aerosols exert major impacts on the Earth's radiative balance, directly by scattering and absorbing solar radiation (1) and indirectly by serving as cloud condensation nuclei (CCN) and influencing cloud properties (2). As the largest emitter of BB aerosols, southern Africa contributes ∼30% of global BB aerosols by mass (3). From July though October, a large portion of these BB aerosols are transported by the predominant circulation over the southeastern Atlantic Ocean (SEA) (4), and interact with the underlying stratocumulus deck (5). The SEA stratocumulus deck in this region is semipermanent and very important for global climate, because these clouds reflect a significant amount of solar radiation and exert only a small radiative effect in the longwave. Modest changes in cloud coverage (15–20% increase) or liquid water path (20–35% increase) are able to generate a radiative effect that is comparable, but of opposite sign, to those caused by increasing greenhouse gases (6).

The fire season in southern Africa just partly coincides with the season of maximum cloud coverage over SEA, which constitutes Earth's most prominent region of above-cloud aerosols (ACA) (7, 8). Over the ocean, partially absorbing BB aerosols are able to exert either a positive (warming) or negative (cooling) shortwave direct radiative effect (DRE) at the top of atmosphere (TOA), depending on the brightness of the underlying layer (e.g., ocean surface or marine boundary layer [MBL] clouds). Despite many efforts (9–13), there is still no consensus on the magnitude or even the sign of the all-sky DRE of BB aerosols over this region—the modeled annual mean DRE of BB aerosols shows a large spread from −1 to +2 W m^{-2} (12, 14). Some studies, such as ref. 15, report mean instantaneous above-cloud aerosol DRE of around +30 to +35 W m^{-2} in the fire season (August and September). The thermodynamic structure change induced by BB aerosol heating can further trigger cloud adjustment (known as the semidirect effect), namely through a higher tropospheric stability, resulting in a higher cloud liquid water path (LWP) and cloud fraction (CF) of MBL clouds (16–19). The results from general circulation model (GCM) simulations conducted by ref. 19 suggest that, over a large area of the SEA during the fire season (July to October), the sign of the semidirect effect is negative overall, while the magnitude is comparable to the DRE, yielding a total negative radiative effect

Significance

Each year biomass burning (BB) aerosols emitted in southern Africa during the fire season (July–October) transport westward over the southeast Atlantic Ocean and interact with underlying stratocumulus decks. Previous studies showed that BB aerosols greatly perturb the top of atmosphere radiation balance by scattering and absorbing solar radiation and by altering cloud properties via changing the lower tropospheric stability (direct and semidirect effects). Using a state-of-the-art model in combination with satellite observations, we found that BB aerosols that are entrained into the clouds function as cloud condensation nuclei, and increase the brightness of stratocumulus clouds (indirect effect). In these models, this indirect effect dominates the direct and semidirect effects of BB aerosols over this region.

Author contributions: Z.L., X.L., and Z.Z. designed research; Z.L., X.L., and Z.Z. performed research; Z.L., Z.Z., C.Z., K.M., C.R., C.W., and Z.Y. analyzed data; and Z.L., X.L., and J.E.P. wrote the paper.

The authors declare no conflict of interest.

This article is a PNAS Direct Submission. J.H. is a guest editor invited by the Editorial Board.

[1]To whom correspondence should be addressed. Email: xliu6@uwyo.edu.

This article contains supporting information online at www.pnas.org/lookup/suppl/doi:10.1073/pnas.1713703115/-/DCSupplemental.

Published online March 5, 2018.

(DRE plus semidirect effect) of −0.8 to −1.7 W m^{-2}. In addition, the moisture within smoke plumes can reduce cloud-top longwave cooling and cloud water path (20, 21).

Compared with the DRE and semidirect effect of BB aerosols, the effect of CCN activated from BB aerosols (known as the microphysical effect) on MBL clouds over the SEA has received less attention, because previously it was thought that BB aerosol plumes in this region are well separated from the underlying cloud layers (5, 18). Recent satellite observational studies suggested the possible effect of BB aerosols on changing cloud properties via functioning as CCN (22–24). However, direct evidence showing that the SEA BB aerosols are in contact with the underlying MBL clouds and function as CCN is still limited.

A relatively new lidar installed on the International Space Station (ISS) called the Cloud-Aerosol Transport System (CATS) began operating in January 2015 (25). The use of a 1,064-nm lidar enables CATS to detect the full vertical extent of ACA in comparison with the Cloud-Aerosol Lidar with Orthogonal Polarization (CALIOP) that uses the 532-nm wavelength which, due to strong aerosol absorption, often cannot detect the lower portions of optically thicker ACA layers; thus CALIOP tends to place the ACA base at higher altitudes, implying that ACA are well separated from the underlying clouds (24, 26, 27). As shown in Fig. 1, however, an analysis of the CATS nighttime vertical feature mask products over SEA during the fire seasons of 2015 and 2016 (August to September) shows that close to 50% of ACA cases on average over both coastal (coast 2° to 17°S, [around 14°E] to 0°) and remote regions (2° to 17°S, 0° to 17°W) actually have the aerosol layer adjacent to cloud top (i.e., the distance between the ACA base and the cloud top is smaller than 60 m, which is the vertical resolution of CATS). This result suggests that BB aerosols may likely contact and alter the cloud by serving as CCN quickly after they are transported over SEA.

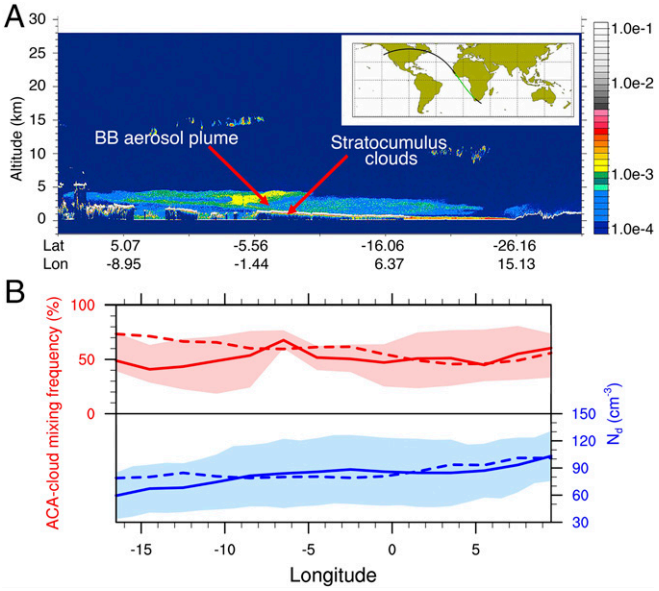

Fig. 1. (*A*) BB aerosol plume in contact with underlying MBL clouds. The figure shows 1,064-nm total attenuated backscatter (km^{-1} sr^{-1}, per kilometer per steradian) as observed by CATS from 0441:44 to 0455:36 UTC, August 5, 2015. The path of ISS is shown as a green line in the superimposed map. Images courtesy of The NASA CATS-ISS project. (*B*) The red solid and dashed lines show ACA–cloud mixing frequency observed by CATS and modeled by WRF-Chem (i.e., the frequency of ACA cases with aerosol in contact with cloud top) as a function of longitude during the fire seasons (August–September 2014, for modeled frequency and August–September 2015 and 2016 for observed frequency). The blue solid and dashed lines represent the meridional distributions of N_d as observed by MODIS/Aqua and modeled by WRF-Chem model over the study domain during the fire season (August–September 2014), respectively. The shaded area in *B,* Upper, represents the maximum and minimum range of monthly ACA–cloud mixing frequency observed by CATS for August–September 2015 and 2016, while the shaded area in the *B,* Lower, represents the SDs of daily N_d as observed by MODIS/Aqua.

Aerosols are usually released and activated as CCN in the boundary layer below clouds. All else equal, an increase of CCN increases cloud droplet number concentrations (N_d) and suppresses surface precipitation. In the SEA, these changes occur after BB aerosols have entered the MBL, either through entrainment from the cloud top or advection off the African continent and entrainment from below clouds. A few recent studies tried to use satellite observations to assess the aerosol microphysical effects exerted by BB aerosols in the SEA (23, 24). However, because of the covariation of aerosols and meteorology, it is hard to determine the aerosol effects on MBL clouds solely from observations, and even more challenging to quantify the relative importance of the microphysical effects, which are inherently entangled with semidirect effects. In addition, the aerosol microphysical effects on MBL clouds may vary strongly within a day because the MBL clouds exhibit strong diurnal cycles through coupling (during the night) and decoupling (during the day) processes (6). Therefore, to unravel the dominating mechanisms, it is also critical to examine the diurnal variation of aerosol microphysical effects.

Cloud-top entrainment describes the mixing between cloud and dry air that occurs at cloud top that influences cloud-top height and cloud-top microphysics. If cloud droplet number concentrations increase, without a corresponding increase in LWP, entrainment can increase on a time scale comparable with the eddy turnover time scale (1 h or less) because faster evaporation of the smaller cloud drops at cloud top can decrease temperatures enhancing turnover of eddies. In turn, the enhanced entrainment can cause the stratocumulus-topped boundary layer (STBL) to warm and dry, thereby reducing CF and LWP on a time scale that is markedly longer (6). Due to such complex negative feedbacks, previous studies have found that the aerosol microphysical effects on clouds may be diminished or even cancelled under some scenarios [e.g., in cases with small precipitation but strong entrainment (28) or with relatively high cloud base (29)]. Therefore, it is critical to assess the total net microphysical effect of BB aerosols over the SEA during the fire season using a model that can account for all of the relevant cloud processes in these scenarios. Due to the complex interactions between microphysics, radiation, turbulence, and entrainment processes associated with MBL clouds (30), simulating MBL clouds has proven to be a challenging task, especially in GCMs (6). Over the SEA, 12 models employed in the Intergovernmental Panel on Climate Change (IPCC) Fifth Assessment Report (AR5) underestimate the magnitude of annual mean shortwave cloud radiative forcing by 10–20 W m^{-2} (31). This large discrepancy motivates us to use high-resolution models instead of GCMs with coarser resolutions to study the effect of BB aerosols on MBL clouds.

In this work, we use advanced modeling techniques (large eddy simulations [LES] nested within Weather Research and Forecasting with Chemistry [WRF-Chem]) to study the role of BB aerosols in regulating the properties of MBL clouds and the resulting radiative energy budget in the SEA, with a specific focus on the relative importance between the semidirect and microphysical effects. In WRF-Chem, 2-mo simulations from August 1 to September 30, 2014, are conducted at a convection-permitting scale of 3 km in three contrasting aerosol scenarios, namely a case with only sea salt and DMS emissions (clean or "C" case), a case with BB aerosol, sea salt, and DMS emissions (polluted or "P" case), and a case similar to P case, but with the radiative effect of biomass aerosols turned off and with only the microphysical effect of aerosols on clouds included (microphysics only or "M" case). The difference between the P and C cases

is a measure of the total effect of BB aerosols, whereas the difference between the P and M cases represents the sum of direct and semidirect effects of BB aerosols. In addition, we also conduct WRF-LES simulations to corroborate the performance of WRF-Chem. All of the WRF-LES domains have 97 (vertical levels) × 500 × 500 model grids with horizontal resolutions of 66.7 m and 52 layers from 0 to 1 km and 25 layers from 1 to 2 km. In both WRF-Chem and WRF-LES, the Morrison two-moment cloud microphysical scheme is adopted to treat sophisticated aerosol–cloud interactions.

Evaluation of WRF-Chem Against Satellite Observations

Before examining the impact of BB aerosols on stratocumulus clouds, we thoroughly evaluate the WRF-Chem performance by comparing aerosol and cloud fields from the P case against the Moderate Resolution Imaging Spectroradiometer (MODIS), CALIOP, and CATS observations over the SEA. We found an excellent agreement between modeled and observed above-cloud aerosol optical depth (AOD), in terms of both domain-averaged values (0.357 from MODIS on the Aqua satellite vs. 0.351 from P case) and spatial distributions as shown in the *SI Appendix*, Fig. S1 *A* and *B*. Above-cloud AODs, in both the model simulation and MODIS retrievals, peak near the coast between 5° and 10°S, and gradually decrease westward. This agreement lends confidence to our simulation of the BB aerosol emission and horizontal transport. We further evaluate the modeled frequency of occurrence of ACA cases with aerosol in contact with cloud top (ACA–cloud mixing frequency) as a function of longitude (Fig. 1*B*), which is generally in good agreement with the CATS observations, although the model tends to predict higher mixing frequencies over 10° to 17°W. The discrepancy in ACA–cloud mixing frequency between model and observation may be also due to relatively low sampling rates of ACA by CATS over this region, where the stratocumulus-to-cumulus transition occurs. Over this region, the model predicted N_d is about 15 cm^{-3} higher compared with the MODIS/Aqua retrievals (32) as shown in Fig. 1*B*; whereas, over other regions, the model has a good performance.

SI Appendix, Fig. S1*C* shows the vertical distribution of aerosols observed by the spaceborne lidars CALIOP and CATS over the coastal and remote regions during nighttime averaged over the fire season (August–September of 2014 for CALIOP and August–September 2015 and 2016 for CATS). A comparison of the vertical profiles reveals that, when transporting westward from the coastal region to the remote region, BB aerosols gradually descend to lower altitudes, likely because of large-scale subsidence and/or gravitational settling. A comparison of modeled (*SI Appendix*, Fig. S1*D*) with observed vertical profiles (*SI Appendix*, Fig. S1*C*) shows that WRF-Chem reasonably captures the transition of vertical distributions of aerosol features from the coastal to remote region. *SI Appendix*, Fig. S1 *C* and *D* also shows the relative occurrence frequencies of cloud-top heights over the SEA as (*SI Appendix*, Fig. S1*C*) observed by CALIOP and (*SI Appendix*, Fig. S1*D*) modeled by the P case and C case during the daytime of the study period. Model simulations for the P case depict a very similar picture although the cloud-top heights are slightly underestimated.

SI Appendix, Table S1 shows the aerosol and cloud properties modeled by the three cases and the corresponding satellite measurements/retrievals averaged over the SEA and study period, including CF, LWP, cloud-top N_d, and ACA occurrence frequency (See *SI Appendix*, Figs. S2 and S3, for the spatial distributions of these properties). Uncertainties associated with satellite measurements are discussed in the *SI Appendix*. All these model-simulated parameters are in good agreement with the satellite observations.

Effect of BB Aerosols on Stratocumulus Clouds

Fig. 2*A* shows the diurnal changes of modeled N_d averaged over the SEA. The P and M cases predict a domain average of about 100 cm^{-3} of N_d through the entire day (N_d is slightly lower during the daytime); whereas, the C case predicts about half of N_d compared with the other two cases. In contrast, modeled cloud LWP, cloud optical depth (τ_c), and CF fields averaged over the SEA for the study period exhibit strong diurnal cycles, which peak at 0600 UTC and decrease to a minimum at 1500 UTC as shown in Fig. 2 *B*–*D*. Due to the microphysical effect of BB aerosols, MBL clouds in the P case tend to have higher cloud LWP than their counterparts in the C case throughout the day, especially during the early morning hours (0600 UTC). By the afternoon (1200–1500 UTC), the difference in LWP (ΔLWP, Δ denotes the difference in cloud properties between P case and C case) reduces to 5.2 g m^{-2}. The diurnal cycles of τ_c closely follow those of LWP; however, because of higher N_d (the Twomey effect) in the P case, the relative increases in τ_c due to BB aerosols (by about 25–30%) are much larger than the increases due to LWP (<10%). Therefore, the BB aerosols are able to increase the brightness of stratocumulus clouds significantly over the SEA during the fire season.

As shown in Fig. 2*D*, BB aerosols can enhance the amplitude of the CF diurnal cycle, as the P case predicts 2.1% higher CF during the early morning and 2.0% lower CF during the afternoon compared with the C case. In addition to two snapshots of MODIS observations, the modeled CF diurnal cycles also lie within the range of time series of CF as observed by Spinning Enhanced Visible and Infrared Imager (SEVIRI) (33). In Fig. 2 *E* and *F*, the solid lines marked with blue circles show ΔCF over the coastal and remote regions, respectively. During the morning, both regions experience more than a 2% increase in CF under the influence of BB aerosols. After 1200 UTC, the P case

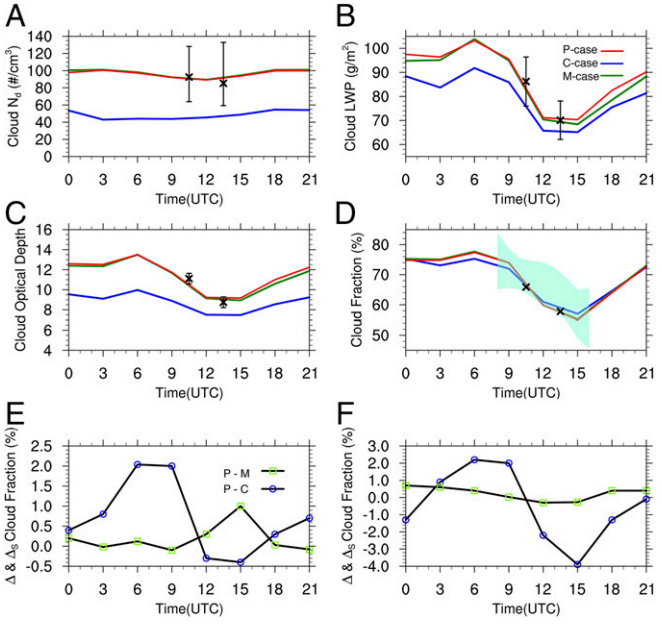

Fig. 2. Diurnal cycles of (*A*) N_d, (*B*) cloud LWP, (*C*) cloud optical depth, and (*D*) CF modeled by P case (red line), C case (blue line), and M case (green line) over SEA; CF differences between P case and C case (line with blue circle) and between P case and M case (line with green square) over (*E*) the coastal and (*F*) the remote regions, respectively. The black crosses on *A*–*D* represents the values observed by MODIS/Terra and MODIS/Aqua. The error bars are derived from the time series of domain-averaged uncertainties of MODIS cloud properties. Light-green shaded area in *D* represents the ranges of CF as observed by SEVIRI.

predicts nearly 4% lower CF than the C case over the remote region; whereas, there is only a slightly lower CF (<1%) over the coastal region. This result is consistent with the microphysical effect of BB aerosols that first causes higher LWP due to precipitation suppression (28) (*SI Appendix*, Fig. S4) and stronger entrainment due to higher LWP and N_d (faster evaporative cooling at cloud top) before noon. Later, higher entrainment rates are able to reduce the magnitude of LWP increase and enhance the breakup of stratocumulus clouds during the afternoon, especially over the remote region. (In the afternoon, ΔLWP remains positive over a large area of the SEA, and only becomes negative over a relative small area of the remote region. See *SI Appendix*, Fig. S5 for more detailed analysis of the spatial pattern of ΔLWP.) Another plausible reason for significantly reduced CF over the remote region during the afternoon is that the higher entrainment rate from night to early morning deepens the MBL (e.g., higher cloud top), making it more prone to decoupling from surface moisture supply during the day. Therefore, there is a delayed impact leading to an earlier transition into trade cumulus in the remote region. The decoupling occurs more frequent during the day than the night. The process is discussed more in detail in *SI Appendix*.

In Fig. 2 *E* and *F*, the solid lines marked with green squares represent the difference in CF between the P case and M case (Δ_SCF, Δ_S denotes the difference in cloud properties between P case and M case due to the semidirect effect) over the coastal and remote regions, respectively. We find that the semidirect effect of BB aerosols only plays a significant role over the coastal region during the afternoon by increasing lower tropospheric stability (LTS) and cloud fraction (Δ_SCF ~ 1%). Over this region, consistent with the findings in ref. 19, because of the large CF, dense BB aerosol layers are able to produce a strong semidirect effect (a negative radiative effect), partially preventing the breakup of cloud decks during the afternoon due to entrainment. We further examined the impacts of BB aerosols on the diurnal cycles of CF and LWP modeled by the WRF-LES model (*SI Appendix*, Figs. S6 and S7), which agrees reasonably with the WRF-Chem results in Fig. 2.

A comparison of the cloud-top heights between the P and C cases in *SI Appendix*, Fig. S1*D* shows that an important effect of above-cloud BB aerosols is to enhance the mean cloud-top height over the SEA by 45–50 m during the daytime in the 2-d reinitialized simulations, partially owing to stronger cloud-top entrainment rates in the P case (34). (The diurnal cycles of cloud-top heights modeled by three cases are shown in *SI Appendix*, Fig. S8.) In addition, by conducting a group of short-period WRF-Chem simulations (10 d, from September 1 to 11, 2014) and performing a budget analysis with a passive tracer (34), we confirm that the P case, compared with the C case, produces higher cloud-top entrainment rates (3.4 vs. 2.1 mm s^{-1}, daily mean), which can be interpreted as enhanced local mixing in the WRF-Chem model (see details in ref. 34).

In Fig. 3, we examine the radiative forcing caused by the BB aerosols over the SEA. In the scatterplot, modeled upward shortwave (SW) fluxes at TOA ($SW_{TOA}\uparrow$) are compared against Clouds and the Earth's Radiant Energy System (CERES) observations averaged over 0900, 1200, and 1500 UTC of each day. Both the regression slope and the correlation coefficient suggest $SW_{TOA}\uparrow$ modeled by the P case is in better agreement with CERES retrievals than the C case. On average, the P case slightly overestimates $SW_{TOA}\uparrow$ by 1.6 W m^{-2}, and the C case underestimates $SW_{TOA}\uparrow$ by 18.4 W m^{-2}. As shown in Table 1, the difference in daily mean $SW_{TOA}\uparrow$ between the P case and C case is as high as 8.05 W m^{-2}, a cooling effect that is mostly caused by the microphysical effect of BB aerosols on clouds (−7.01 W m^{-2}, the difference between the M case and C case), and also contributed by the DRE and semidirect effects (a combined effect of −1.04 W m^{-2}, the difference between the P case and M case). Because of higher N_d and LWP during the daytime and higher CF before noon, the microphysical effect of BB aerosols causes a strong cooling over both the coastal and remote regions (−8.28 and −6.12 W m^{-2}) as shown in Table 1. Following the approach in ref. 35, we estimate the contributions from the BB aerosol-induced changes in N_d, LWP, and CF to the changes in $SW_{TOA}\uparrow$ between M case and C case (the microphysical effect). The results show that the contribution from higher N_d (Twomey effect) is 77.86%, followed by higher LWP (21.09%) and higher CF before noon (1.05%) (cloud lifetime effect, see *SI Appendix* for more details).

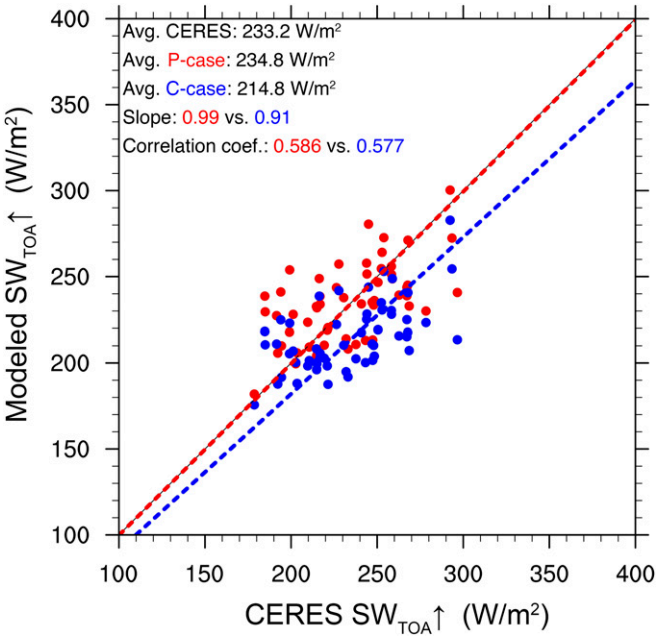

Fig. 3. Scatterplot of modeled $SW_{TOA}\uparrow$ vs. CERES $SW_{TOA}\uparrow$ observations. Each point represents the value averaged over 0900, 1200, and 1500 UTC for each day of the study period. The regression slope is set to pass the (0, 0) point. According to a Student's *t* test, the difference between P case and C case is significant at the 0.01% level.

Over the coast, the sum of direct and semidirect effects of BB aerosols varies from 11.9 W m^{-2} at 0900 UTC to 3.7 W m^{-2} at 1200 UTC to −4.5 W m^{-2} at 1500 UTC. The warming is mainly due to the direct effect of BB aerosols before noon when the CF is relatively large (11). The cooling effect at 1500 UTC is caused by the semidirect effect, which increases the CF by about 1% near the coast as shown in Fig. 2*E*. The daily average sum of the direct and semidirect effects exerts a warming of 1.40 W m^{-2} over the coastal region and a cooling of −2.81 W m^{-2} over the remote region, with an average of −1.04 W m^{-2} over the SEA. This magnitude is comparable to the estimate of −1.7 to −0.8 W m^{-2} in ref. 19 (see *SI Appendix* for comparisons of heating profile and changes in subsidence and LTS due to BB aerosols). The much

Table 1. The daily mean values of cloud microphysical effect and the sum of aerosol direct and semidirect effects caused by BB aerosols over coastal and remote regions, as well as over the entire SEA study domain (Unit: W m^{-2})

Aerosol effects	SEA domain	Coastal region	Remote region
Total effect	−8.05 (−20.0)	−6.88 (−18.0)	−8.93 (−21.6)
Microphysical effect	−7.01 (−18.6)	−8.28 (−21.7)	−6.12 (−16.5)
Direct + semidirect effects	−1.04 (−1.4)	+1.40 (+3.7)	−2.81 (−5.1)

The values in parentheses are averaged over 9 UTC, 12 UTC, and 15 UTC of the study period.

larger cooling associated with the microphysical effect, especially the Twomey effect of BB aerosols on clouds is the dominant factor in determining the total radiative forcing at TOA, and further highlights the need for reasonably representing the microphysical effect of BB aerosols on clouds over the SEA in climate models (31).

Discussion

In this study, we employed the WRF-Chem/WRF-LES models in conjunction with satellite observations to study the effects of BB aerosols emitted from southern African fires on stratocumulus clouds and the radiative energy budget over the southeast Atlantic Ocean. The main findings of the impact of BB aerosols on the diurnal cycle of clouds are schematically summarized in Fig. 4. We find that, over the entire SEA domain in both day and night, BB aerosols are entrained into clouds from above, function as CCN, and increase N_d and cloud brightness, leading to a negative radiative effect that dominates over the direct and semidirect effects of the aerosol. During the late nighttime to earlier morning, the microphysical effect of BB aerosols increases cloud LWP and CF by reducing drizzle formation. Higher N_d and LWP increase the cloud-top height and entrainment rate at cloud top. Due to stronger entrainment, the changes in cloud LWP due to BB aerosols remain positive but reduce in magnitude, while the changes in CF switch from positive to negative in the afternoon. Another plausible reason is that the deeper MBL caused by higher entrainment during the night makes it more prone to decoupling during the day.

Near the coastal region where CF is large, the semidirect effect of BB aerosols partially counteracts the microphysical effect on the reduction of CF in the afternoon. Thus, the net effect of BB aerosols on CF over the coastal region is slightly negative (by −0.5%) during the afternoon, whereas CF over the remote region is significantly reduced (by −4%) under the influence of BB aerosols. Therefore, by increasing cloud brightness with higher N_d and LWP during the daytime and higher CF during the morning, the microphysical effect of biomass smoke can cause a significant cooling at TOA, bringing the domain averaged $SW_{TOA}\uparrow$ modeled by the P case into much better agreement with CERES observations than the C case. In addition to BB aerosol-induced changes in SW radiative energy budget discussed above, fire events in southern Africa are also able to alter longwave (LW) radiative energy budget over SEA. For instance, the moisture within BB aerosol plumes has a potentially important effect on cloud-top LW cooling over SEA (21), which is not discussed in this study.

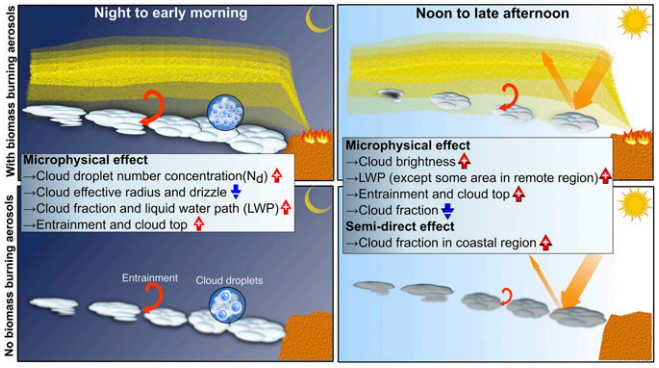

Fig. 4. Schematic illustration of the main findings of this study. *Upper* shows the case with BB aerosols during the night to early morning (*Left*) and noon to late afternoon (*Right*) periods. Similarly shown in *Lower* is the case with no BB aerosols during the same periods.

Although we have compared and evaluated our modeled aerosol and cloud fields against satellite observations whenever possible, two important aspects of simulations are still not constrained by observations due to the lack of data. As pointed out in many previous studies, the DRE of BB aerosols is strongly dependent upon their single scattering albedo (SSA). However, estimating the SSA from remote sensing observations is challenging. As a result, there is still a lack of reliable observations to validate the scattering properties of BB aerosols used in our DRE computations. Another aspect is the exact amount of BB aerosols entrained into the clouds, which directly influences the magnitude of the cloud microphysical effects. However, it is extremely difficult, if not impossible, to estimate the amount of entrained aerosols from satellite observations. Fortunately, in 2016, several international and multiagency field campaigns, including Observations of Aerosols Above Clouds and Their Interactions (ORACLES) and Layered Atlantic Smoke Interactions with Clouds (LASIC), were conducted over southern Africa and the SEA; some of these campaigns have resumed in 2017 [in addition to Cloud–Aerosol–Radiation Interactions and Forcing (CLARIFY) and Aerosol Radiation and Clouds in southern Africa (AEROCLO-Sa)] and are scheduled to continue in 2018. The main goals of these campaigns are to characterize the radiative and microphysical effects of BB aerosols on cloud properties, etc. With abundant in situ measurement incorporated in our model simulations, we hope to more accurately assess the effects of BB aerosols on stratocumulus clouds over this region. Even with the above uncertainties, however, based on the high ACA–cloud mixing frequency observed by CATS, our model simulations indicate strong evidence that BB aerosols are able to significantly enhance cloud N_d and LWP, and hence τ_c and the brightness of stratocumulus over SEA.

Our results change what we know about the impacts of BB aerosols on the regional radiative balance over SEA. Nearly all previous studies focused on estimating the direct and semidirect effects of BB aerosols; however, the magnitudes of these two effects (−2 to 2 W m^{-2}) are much smaller than the microphysical effect of BB aerosols (−7.01 W m^{-2}) estimated in this study. Therefore, missing or incorrect representations of this strong cooling effect can contribute to the underestimation of shortwave cloud radiative forcing calculated by GCMs in this region. Furthermore, despite the fact that our study focused on the radiative energy budget over the SEA region only, the results have broad implications for global climate system. First, a cooling of −8.05 W m^{-2} over SEA in our study domain can be roughly translated to global cooling of −0.089 W m^{-2} during the fire season. This cooling effect is significant and comparable to the radiative forcing from many other forcing agents assessed in IPCC AR5 [e.g., the radiative forcing due to aerosol–radiation interactions as estimated by IPCC AR5 is −0.35 W m^{-2} (1)]. Second, this study emphasizes the importance of studying the competing effects between aerosol–radiation and aerosol–cloud interactions in other geographical regions (e.g., in the Arctic), where BB aerosols often coexist with stratocumulus.

Methods

We first use the Weather Research and Forecasting with Chemistry (WRF-Chem) model version 3.6.1 (36) to simulate the transport of BB aerosols from the African continent and their interaction with underlying MBL clouds over coastal and remote oceanic regions. The simulation domain covers a vast region of 6,000 km (longitudinal direction) × 1,800 km (latitudinal direction) including southern Africa and the southeast Atlantic Ocean. We conduct a series of 3-d forecasts at a horizontal resolution of 3 km by simulating the chemistry continuously from August 1 to September 30, 2014, but reinitializing meteorological initial and boundary conditions and sea surface temperatures with the National Centers for Environmental Prediction (NCEP) Final (FNL) reanalysis data every 2 d. The first day of each 3-d simulation is used as a spin-up period and only the results of the last 2 d are used for analysis. By reinitializing meteorology every 2 d, we do not

consider the feedbacks of aerosol on large-scale circulation, but fast processes, such as aerosol interactions with radiation and clouds, LTS, and subsidence are accounted for in the model simulations. The hourly BB aerosol emissions are generated from SEVIRI satellite observations of fire radiative power. (See *SI Appendix* for more details.)

By comparing the results of the P case against the C case and M case, we are able to quantify the total effects (direct + semidirect + microphysical effects) and direct + semidirect effects of BB aerosols, respectively. To corroborate the WRF-Chem results, we run the nested WRF model in the large-eddy simulation mode (37) at a horizontal resolution with the innermost nest of 66.7 m over four subdomains centered over SEA, driven by the meteorology and aerosol fields modeled by WRF-Chem. (See *SI Appendix* for more details on WRF-Chem and WRF-LES model configurations.) Modeled aerosol and cloud fields are compared and evaluated against satellite observations whenever possible. (See *SI Appendix* for more details on the description of satellite data.) The differences in cloud properties and shortwave fluxes at TOA between different aerosol scenarios aid in the interpretation of the semidirect and microphysical effects of BB aerosols on cloud properties and the radiative energy budget.

ACKNOWLEDGMENTS. This work was supported by the Office of Science of the US Department of Energy (DOE) as the National Science Foundation (NSF)-DOE-US Department of Agriculture Joint Earth System Modeling (EaSM) Program and the Earth System Modeling Program. The authors would like to acknowledge the use of computational resources (ark:/85065/d7wd3xhc) at the National Center for Atmospheric Research (NCAR)-Wyoming Supercomputing Center provided by the National Science Foundation and the State of Wyoming, and supported by NCAR's Computational and Information Systems Laboratory. Z.Z.'s research is partly supported by National Aeronautics and Space Administration (NASA) Grant NNX14AI35G and DOE Grant DE-SC0014641. C.Z. is supported by the "Thousand Talents Plan for Young Professionals" program of China. K.M.'s work is supported by the NASA CloudSat and CALIPSO Science Team Grant NNH14CK44C and the NASA Radiation Sciences Program.

1. Myhre G, et al. (2013) Anthropogenic and natural radiative forcing. *Climate Change 2013: The Physical Science Basis. Contribution of Working Group I to the Fifth Assessment Report of the Intergovernmental Panel on Climate Change*, eds Stocker TF, et al. (Cambridge Univ Press, Cambridge, UK), pp 659–740.
2. Boucher O, et al. (2013) Clouds and aerosols. *Climate Change 2013: The Physical Science Basis. Contribution of Working Group I to the Fifth Assessment Report of the Intergovernmental Panel on Climate Change*, eds Stocker TF, et al. (Cambridge Univ Press, Cambridge, UK).
3. Van der Werf GR, et al. (2010) Global fire emissions and the contribution of deforestation, savanna, forest, agricultural, and peat fires (1997–2009). *Atmos Chem Phys* 10:11707–11735.
4. Adebiyi AA, Zuidema P (2016) The role of the southern African easterly jet in modifying the southeast Atlantic aerosol and cloud environments. *Q J R Meteorol Soc* 142: 1574–1589.
5. Hobbs PV (2002) Atmosphere science: Clean air slots amid atmospheric pollution. *Nature* 415:861.
6. Wood R (2012) Stratocumulus clouds. *Mon Weather Rev* 140:2373–2423.
7. Devasthale A, Thomas MA (2011) A global survey of aerosol-liquid water cloud overlap based on four years of CALIPSO-CALIOP data. *Atmos Chem Phys* 11: 1143–1154.
8. Waquet F, et al. (2013) Global analysis of aerosol properties above clouds. *Geophys Res Lett* 40:5809–5814.
9. Zhang Z, et al. (2016) Shortwave direct radiative effects of above-cloud aerosols over global oceans derived from 8 years of CALIOP and MODIS observations. *Atmos Chem Phys* 16:2877–2900.
10. Schulz M, et al. (2006) Radiative forcing by aerosols as derived from the AeroCom present-day and pre-industrial simulations. *Atmos Chem Phys* 6:5225–5246.
11. Chand D, Wood R, Anderson TL, Satheesh SK, Charlson RJ (2009) Satellite-derived direct radiative effect of aerosols dependent on cloud cover. *Nat Geosci* 2:181–184.
12. Stier P, et al. (2013) Host model uncertainties in aerosol radiative forcing estimates: Results from the AeroCom prescribed intercomparison study. *Atmos Chem Phys* 13: 3245–3270.
13. Meyer K, Platnick S, Oreopoulos L, Lee D (2013) Estimating the direct radiative effect of absorbing aerosols overlying marine boundary layer clouds in the southeast Atlantic using MODIS and CALIOP. *J Geophys Res Atmos* 118:4801–4815.
14. Zuidema P, et al. (2016) Smoke and clouds above the southeast Atlantic: Upcoming field campaigns probe absorbing aerosol's impact on climate. *Bull Am Meteorol Soc* 97:1131–1135.
15. de Graaf M, Bellouin N, Tilstra LG, Haywood J, Stammes P (2014) Aerosol direct radiative effect of smoke over clouds over the southeast Atlantic Ocean from 2006 to 2009. *Geophys Res Lett* 41:7723–7730.
16. Penner JE, Zhang SY, Chuang CC (2003) Soot and smoke aerosol may not warm climate. *J Geophys Res Atmos* 108:4657.
17. Johnson B, Shine K, Forster P (2004) The semi-direct aerosol effect: Impact of absorbing aerosols on marine stratocumulus. *Q J R Meteorol Soc* 130:1407–1422.
18. Wilcox E (2012) Direct and semi-direct radiative forcing of smoke aerosols over clouds. *Atmos Chem Phys* 12:139–149.
19. Sakaeda N, Wood R, Rasch PJ (2011) Direct and semidirect aerosol effects of southern African biomass burning aerosol. *J Geophys Res Atmos* 116:D12205.
20. Yamaguchi T, Feingold G, Kazil J, McComiskey A (2015) Stratocumulus to cumulus transition in the presence of elevated smoke layers. *Geophys Res Lett* 42: 10478–10485.
21. Adebiyi AA, Zuidema P, Abel SJ (2015) The convolution of dynamics and moisture with the presence of shortwave absorbing aerosols over the southeast Atlantic. *J Clim* 28:1997–2024.
22. Costantino L, Bréon FM (2010) Analysis of aerosol-cloud interaction from multi-sensor satellite observations. *Geophys Res Lett* 37:L11801.
23. Costantino L, Bréon F-M (2013) Aerosol indirect effect on warm clouds over South-East Atlantic from co-located MODIS and CALIPSO observations. *Atmos Chem Phys* 13: 69–88.
24. Painemal D, Kato S, Minnis P (2014) Boundary layer regulation in the southeast Atlantic cloud microphysics during the biomass burning season as seen by the A-train satellite constellation. *J Geophys Res Atmos* 119:11288–11302.
25. Yorks J, et al. (2016) An overview of the CATS level 1 processing algorithms and data products. *Geophys Res Lett* 43:4632–4639.
26. Vaughan MA, et al. (2009) Fully automated detection of cloud and aerosol layers in the CALIPSO lidar measurements. *J Atmos Ocean Technol* 26:2034–2050.
27. Rajapakshe C, et al. (2007) Seasonally transported aerosol layers over southeast Atlantic are closer to underlying clouds than previously reported. *Geophys Res Lett* 44: 5818–5825.
28. Ackerman AS, Kirkpatrick MP, Stevens DE, Toon OB (2004) The impact of humidity above stratiform clouds on indirect aerosol climate forcing. *Nature* 432:1014–1017.
29. Wood R (2007) Cancellation of aerosol indirect effects in marine stratocumulus through cloud thinning. *J Atmos Sci* 64:2657–2669.
30. Zhu P, et al. (2005) Intercomparison and interpretation of single-column model simulations of a nocturnal stratocumulus-topped marine boundary layer. *Mon Weather Rev* 133:2741–2758.
31. Flato G, et al. (2013) Evaluation of climate models. *Climate Change 2013: The Physical Science Basis. Contribution of Working Group I to the Fifth Assessment Report of the Intergovernmental Panel on Climate Change* (Cambridge Univ Press, Cambridge, UK).
32. George RC, Wood R (2010) Subseasonal variability of low cloud radiative properties over the southeast Pacific Ocean. *Atmos Chem Phys* 10:4047–4063.
33. Roebeling R, Feijt A, Stammes P (2006) Cloud property retrievals for climate monitoring: Implications of differences between spinning enhanced visible and infrared imager (SEVIRI) on METEOSAT-8 and advanced very high resolution radiometer (AVHRR) on NOAA-17. *J Geophys Res Atmos* 111:D20210.
34. Yang Q, et al. (2012) Impact of natural and anthropogenic aerosols on stratocumulus and precipitation in the southeast Pacific: A regional modelling study using WRF-Chem. *Atmos Chem Phys* 12:8777–8796.
35. Grosvenor DP, Field PR, Hill AA, Shipway BJ (2017) The relative importance of macrophysical and cloud albedo changes for aerosol-induced radiative effects in closed-cell stratocumulus: Insight from the modelling of a case study. *Atmos Chem Phys* 17: 5155–5183.
36. Grell GA, et al. (2005) Fully coupled "online" chemistry within the WRF model. *Atmos Environ* 39:6957–6975.
37. Moeng C, Dudhia J, Klemp J, Sullivan P (2007) Examining two-way grid nesting for large eddy simulation of the PBL using the WRF model. *Mon Weather Rev* 135: 2295–2311.